

# Dynamic Reliability Assessment of PEM Fuel Cell Systems

A. Vasilyev<sup>a</sup>, J. Andrews<sup>b</sup>, S.J. Dunnett<sup>c\*</sup>, L.M. Jackson<sup>c</sup>

<sup>a</sup>WMG, The University of Warwick, Coventry, CV4 7AL, United Kingdom

<sup>b</sup>Resilience Engineering Research Group, The University of Nottingham, University Park, Nottingham, NG7 2RD, United Kingdom

<sup>c</sup>Department of Aeronautical & Automotive Engineering, Loughborough University, Loughborough, LE11 3TU, United Kingdom

- Corresponding author

## Abstract

In this paper, a novel model for the dynamic reliability analysis of a polymer electrolyte membrane fuel cell system is developed to account for multi-state dynamics and ageing. The modelling approach involves the combination of physical and stochastic sub-models with shared variables. The physical model consists of deterministic calculations of the system state described by variables such as temperature, pressure, mass flow rates and voltage output. Additionally, estimated component degradation rates are also taken into account. The non-deterministic model is implemented with stochastic Petri nets which model the failures of the balance of plant components within the fuel cell system. Using this approach, the effects of the operating conditions on the reliability of the system were investigated. Monte Carlo simulations of the process highlighted a clear influence of both purging and load cycles on the longevity of the fuel cell system.

*Keywords:* Fuel Cell, Petri nets, Hybrid modelling, Reliability.

## 1. Introduction

A recently published report on the world's energy status highlighted that despite record amounts of energy been generated from renewable sources, fossil fuel consumption still rose at a high rate [1]. As a result global CO<sub>2</sub> emissions continued to increase which is unacceptable if the targets of the Paris Agreement are ever to be reached [2]. Therefore it is essential to develop efficient and sustainable power generation technologies that will help to shift the global energy landscape away from fossil fuels. One of leading consumers of fossil fuels is transportation. Hence reducing the dependency of transport on such fuels is essential. Electric vehicles (EVs) are the prime candidates for reducing this dependence. Among the different types of EVs, fuel cell-powered vehicles (FCV) have the potential to form the future of energy consumption.

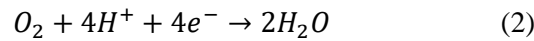
### 1.1. PEM Fuel Cell Technology

Fuel cells (FCs) are a class of power generation devices that use hydrogen fuel to produce electrical power. The output power is the result of the direct transformation of chemical energy stored within the

fuel by an electrochemical process. There are different types of FCs, but in this work polymer electrolyte membrane fuel cells (PEMFC's) are investigated. At the heart of a PEMFC is the polymer membrane, the primary function of which is to conduct protons from the anode to the cathode. At either side of the membrane are catalyst layers that facilitate the chemical reactions. Next to the catalyst are the gas diffusion layers (GDLs) which deliver the reactants to the reaction sites evenly through the diffusion process. The combination of the membrane, catalyst and GDLs forms a single component called the membrane electrode assembly (MEA). The MEA is sandwiched between two bipolar plates, which provide structural backbone to the fuel cell, and supply reactant gases via the gas flow channels embedded in them. The operating principles of a PEMFC is shown in Figure 1. During the fuel cell operation, the hydrogen gas is supplied at the anode electrode. Hydrogen diffuses through the GDL to the anode catalyst layer where the oxidation reaction (Equation 1) releases the electrons ( $e^-$ ) and hydrogen ions ( $H^+$ ).



The released electrons flow to the cathode electrode through an external circuit, thus generating useful work. At the same time, the protons move to the cathode through the membrane. The oxygen (whether as air or pure) supplied to the cathode facilitates the reduction reaction (Equation 2) in which electrons and protons are consumed to create water molecules ( $H_2O$ ) and generate some by-product heat.



Equations 1 and 2 show that the only by-products of the fuel cell operation are water vapour and heat, which is advantageous compared to conventional internal combustion engines.

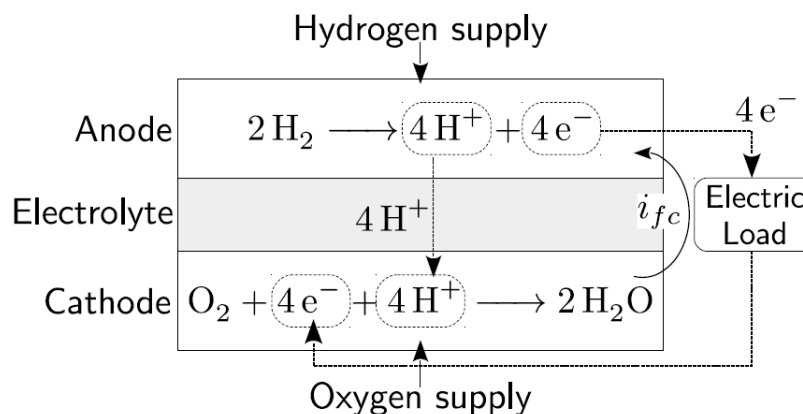


Figure 1: PEM fuel cell operating principle

### 1.2. Balance of plant components

A single PEMFC generates about 1 V, so in order to produce higher voltages, multiple cells are connected in series to create a fuel cell stack. Additional components and sub-systems are required

to create the necessary conditions for efficient FC stack operation. Hydrogen fuel is usually stored in compressed tanks, while air is delivered to the stack from the atmosphere by fans or compressors. The reactant supply sub-systems consists of pipes, valves, mass flow controllers, pressure regulators and filters. Temperature regulation is achieved by either circulating liquid coolant (e.g. water) or air fans or blowers. Gas humidification equipment is also important in order to maintain appropriate levels of water content within the membrane. All the balance of plant components aim to maintain the stack at constant temperature, pressure and humidification with minimized disturbance. Any deviations from a set operating point will lead to decreased stack performance and increased rates of degradation.

### *1.3. PEM Fuel Cell Reliability Issues*

Current generations of PEM fuel cells face a number of issues that limit their lifetime performance. The reliability of the total PEM fuel cell system is determined by the durability of each individual component. For example, membrane degradation affects the membranes ion and water transport properties, catalyst layer deterioration causes the decrease of chemical reaction activity, whilst ageing of the gas diffusion layer hinders the supply of reactants to the reaction sites. In addition to the ageing process, variations in the operating conditions imposed by the auxiliary equipment may accelerate or decelerate the degradation effects. For example, failures in the cooling subsystem may create high temperatures (i.e. above 80 °C) which boosts the reaction kinetics, but, simultaneously, increases the rate of catalyst and membrane degradation [3]. On the other hand, low temperatures facilitate conditions for liquid water accumulation in the gas supply channels and the MEA, which leads to flooding, causing a drop in voltage output. Faults in the reactant supply sub-systems creates reactant starvation, which leads to the creation of local hotspots and further membrane disintegration.

In other words, PEM fuel cell durability is governed not only by natural ageing processes, which cannot be averted, but also by the operating conditions imposed on it by the environment and the supporting equipment [3]. Therefore, reliability of the PEM fuel cell is directly linked to the reliability of the auxiliary equipment and it is crucial to design the system such that the influence of auxiliary equipment failures on the fuel cell stack is minimized. Reliability assessment of PEM fuel cells is important in order to provide estimations for expected lifetime predictions of the system and advise on possible hardware optimizations.

## **2. Literature Review**

### *2.1. Classical Reliability Analysis*

Reliability analysis of any engineering system is a process that requires detailed understanding of all components, their respective functions and the overall goal that the system needs to achieve. Several techniques exist to help perform such analysis, for example Failure Mode and Effects Analysis (FMEA) and Hazard and Operational Analysis (HAZOP). Further investigations into Probabilistic Risk

Analysis can be performed with deductive methods like Fault Trees (FTs) or Event Trees (ETs). Mathematical modelling techniques such as Petri nets (PNs) and simulation can also be applied when reliability of the system depends on sequences and inter-dependencies of various events.

One high-level FMEA was a part of a report by the US Department of Transportation on the safety of compressed hydrogen electrical vehicles [4]. The main objective of the report was to assess the likelihood, criticality and potential consequences of hydrogen leaks occurring in the vehicle. For the purposes of the FMEA, the authors classified the fuel cell components into three functional sub-systems – compressed hydrogen fuel storage, hydrogen flow control and the fuel cell stack. Other authors developed FMEA with the focus on fuel cell components and materials. Wang et al. provides detailed findings on the investigations of the causes and consequences of fuel cell materials degradation [3]. The work classifies the sources of degradation to be associated with internal and external causes. Rama et al. [9] developed an FMEA focussed on the five main causes of performance degradation in PEMFC: activation, ohmic and mass transport losses as well as efficiency deterioration and catastrophic failure. The authors identified 22 potential faults and 47 plausible causes and constructed the corresponding FT to describe the failure interactions. One major limitation of the FMEA approach is the fact that during the analysis only one independent failure mode is considered at a time. When, however, a system is complex and failure modes interact with one another, additional techniques such as Fault Tree Analysis (FTA) are necessary.

The FT approach to reliability assessment of PEMFC's is widely used among researchers in the field. A review paper by Steiner et al. [5] shows how fault tree analysis can be applied to various fuel cell failure modes. The authors presented two fault trees designed to represent flooding or drying of the membrane within PEMFC stacks and also illustrated the application of FTA to understanding the failures encountered in Solid Oxide Fuel Cell (SOFC) systems. However, no numerical evaluations of fault probabilities are provided in this publication. A paper by Placca and Kouta [6] describes the development of a fault tree to model the event 'Degradation of the fuel cell'. This was broken down into three major intermediate events: 'Membrane degradation', 'Catalyst layer degradation' and 'Gas diffusion layers degradation'. These intermediate events were further broken down into more than 40 basic events for which failure data was given. The authors performed 1000 simulations of 100 hours of fuel cell lifetime and concluded that membrane mechanical degradation is the most important intermediate event. This finding agrees with the results of the previously discussed FMEA analysis [4]. One major drawback of this publication is the fact that 100 hours of FC lifetime is negligible when the aim is to ensure that the fuel cells operate for at least 5000 hours. In a publication by Collong and Kouta [7] the authors applied FTA to the safety issues of automotive PEMFC's. They created a FT for 'Tank rupture' and 'Explosion of hydrogen release'. Due to the sparsity of failure rate data for PEMFC systems the authors used data obtained from the offshore reliability data base (OREDA) to quantify the tree. Brik et al. [8] also constructed a fault tree for the top event 'fuel cell system degradation' with

intermediate events ‘auxiliary elements degradation’ and ‘fuel cell degradation’. The authors determined minimal cut sets, minimal combinations of basic events that cause the top event, but emphasised that it is impossible to quantitatively evaluate the top event probability because of the lack of data for all the basic events. Another fault tree analysis carried out by Whiteley et al. [10] showed that the Boolean logic of fault trees is not an ideal method for estimating the probability of fuel cell failure due to complex dependencies of failure modes under differing operating conditions. It was concluded that an alternative method which can deal with such dependencies is necessary.

A modelling technique called Petri Nets (PN’s) is also applicable for reliability analysis and it provides the tools for representation of dependencies, [11]. Several researchers have applied PN’s to the reliability modelling of PEMFC. For instance, Wieland et al. [12] created a simple Petri net for automotive stack degradation and maintenance, multiple assumptions and simplifications were adopted in this model. Degradation modelling by means of Petri nets was carried out by Whiteley et al. [13]. The authors designed various Petri net modules corresponding to various phenomena leading to fuel cell degradation based upon previously conducted FMEA and FTA. The authors concluded that the addition of a fuel cell performance model would improve the simulation results by calculating the evolution of key variables alongside the degradation.

## *2.2. Dynamic Reliability Assessment*

Dynamic Probabilistic Risk Assessment (DPRA) (also called dynamic reliability) is a field of study that aims to expand the classical RAMS techniques by taking into account the multi-state operational and failure mechanisms of the studied system and its changing environmental and operational conditions. A wide range of engineering systems are subject to dynamic operating conditions, so DPRA methods have been applied to a variety of areas: from nuclear safety engineering [14] to structural engineering [15] and rotating machinery [16]. However, the focus in this paper is on DPRA methods designed for complex systems consisting of multiple interacting components within different physical domains.

In principle, such a dynamic approach offers more realistic reliability estimations, but it has not found widespread adoption within industry and remains largely in the domain of academic research due to the complexity of implementation and lack of generalised software tools [17; 18]. The difficulty arises from the fact that DPRA methods aim to capture the inter-dependence and interaction of both deterministic (continuous) and stochastic (discrete) dynamics of the system in order to obtain a more accurate reliability estimates. A formal mathematical definition of systems with such inter-dependencies was established via a class of processes called Piece-wise Deterministic Markov Processes (PDMP) by Davis [19]. Various modelling tools such as Modelica modelling language [20], Matlab/Simulink [21] and Python [22] have been used by research teams to create and analyse PDMP-type models.

Due to the nature of PDMP, it is very difficult to obtain analytical solution, so a sampling approach

such as Monte Carlo (MC) simulations are commonly used to obtain the solution. For example, Bouissou et al. [23] investigated the temperature changes within a room heated by a heater with a constant failure rate  $\lambda=0.01/h$  and a constant repair rate  $\mu=0.1/h$ . The authors implemented this PDMP-type model in Modelica and used MC simulations to obtain a set of temperature trajectories within the room over 100 hours of operation. Lin et al. [24] used Matlab to implement a PDMP model of a pump with inter-dependent degradation mechanisms and employed MC simulations to obtain dynamic reliability curves. The results showed the device reliability sharply decreasing when inter-dependent failures occur. It was also demonstrated how the accuracy of the reliability estimations increases with higher number of MC trials.

In general, there are several methods for implementing the system models suitable for DPRA, each with their own advantages and disadvantages. A comprehensive review of dynamic reliability methods by Shukla and Arul [25] discussed several DPRA methods such as Dynamic Fault Trees (DFT), Petri Nets (PNs), Stochastic Hybrid Automaton (SHA), and several others. The authors also propose a framework for qualitative comparison of these methods and highlight the fact that these methods can be used in conjunction with other modelling tools to represent the complex behaviour of the system.

Taleb-Berrouane et al. [26] propose fusing Bayesian Networks (BNs) with Stochastic Petri Nets (SPNs). In this approach BNs represent the inter-nodal dependencies via conditional probabilities, while SPNs represent dynamic behaviour of the system. The authors use the proposed hybrid methodology to obtain dynamic probability distributions of initiator and intermediate events for pump failure event over 10 years of its operation.

Codetta-Raiteri and Bobbio [27; 28] applied two different types of PNs, Generalised Stochastic Petri Nets (GSPNs) and Fluid Stochastic Petri Nets (FSPN) in the dynamic reliability analysis of a heated tank problem. After performing MC simulations, the authors concluded that both methods provide satisfactory results. However FSPNs allow for greater modelling flexibility, while GSPNs would not be able to handle more complex systems where multiple continuous variables are involved. One drawback of FSPNs is the fact that the ODEs governing the continuous-time evolution of the system must be coded directly into the PN structure. This means that the model code must be written for a specific modelling purpose and cannot be reused in different scenarios.

Manno et al. [29] recognised the fact that when adapting FSPNs and Coloured Petri Nets (CPNs) for DPRA both deterministic and stochastic aspects of the process are fused together and cannot be separated. The authors, thus, suggested to 'separate the concerns' and implement the two aspects of system behaviour independently from each other. The non-deterministic side is represented by a Stochastic Activity Network (SAN), which is another extension of the stochastic PNs. The method was applied to an air conditioning system. Chiacchio et al. [30] continued the analysis of the same system but proposed using Stochastic Hybrid Automaton (SHA) to implement the stochastic events within the system. The SHA is an approach which breaks down a system into a physical and a stochastic model that are coupled together with shared variables and synchronising mechanisms.

Recently, Chiacchio et al. [21] developed a Matlab/Simulink toolbox called SHyFTOO dedicated to solving Stochastic Hybrid Fault Tree Automaton (SHyFTA) problems. The authors deployed this toolbox to study of an electric motor reliability subjected to seasonal variations in ambient temperature. Comparing the device unreliability calculated by using the SHyFTA and conventional FTA revealed that FTA yields lower reliability after the first 9000 hours of motor operation. This is due to the inability of the FTA to consider nonlinear degradation rates of the ball bearing caused by the temperature variations.

Rychkov and Chraibi [31] used a Python based toolbox called PyCATSHOO to study DPRA of the decay heat removal system of a nuclear reactor during the design phase. The MC simulations allowed the researchers to compute a set of temperature trajectories of the sodium coolant and determine which sequence of events leads to the temperature exceeding a critical threshold and calculate the corresponding failure probability.

An alternative way to represent the system for dynamic reliability is through the use of so-called '*smart*' components [18, 25, 32]. The main principle of this approach is to explicitly code both nominal and faulty physical behaviours of individual components within the system. Consequently, system models composed of such fault-augmented components, are inherently suitable for reliability estimations via simulations. One example of using this approach was demonstrated by Schallert [33, 20] who developed a set of fault-augmented models of basic electrical components using an object-oriented modelling language called Modelica. These component models were then used to create a system model of an aeroplane electric network and dispatch reliability over 200 flight hours was calculated to be 0.869. The approach incorporates the capabilities of a classical RAMS technique such as FT's into a physics-based simulation model. The smart component method was also used for nuclear safety by Shukla and Arul [34].

The application of DPRA concepts to reliability assessment of PEMFCs is highly attractive, especially in automotive applications because the degradation rates of the stack depend on the different modes of operation and discrete events such as start/stop cycles. However, to the best of authors knowledge, only one study in this area was published by Fecarotti et al [35]. The authors introduced ideas of DPRA in evaluating the reliability characteristics of PEMFC systems and developed a CPN model of the full FCS containing the fuel cell stack and all the main auxiliary components within its cooling, humidification and gas supply sub-systems. The model also included modelling of maintenance procedures. Performing the model simulations several thousand times provided statistical estimations of the expected lifetime of the system under pre-defined operating conditions and maintenance schedule. The developed CPN model does not take into account the degraded state of the stack due to the changes of operating conditions, resulting in a more static view of system reliability, so a more detailed stack representation is desirable. Additionally, this modelling approach, suffers from the same limitation as FSPN and the code cannot be easily adapted and extended to include some of the more nuanced fuel cell dynamics or even model some other engineering system altogether. The proposed approach can be used for DPRA,

but it suffers from modelling limitations due to the fact that the physical properties of the system have to be interpreted in a modelling paradigm, originally not designed for this use.

To summarise this section, several conclusions can be drawn. Dynamic reliability is an active area of research with a large potential to expand the classical RAMS techniques for analysis of complex engineering systems exhibiting hybrid dynamics. Although various modelling paradigms (e.g. PNs, SHAs and ‘*smart*’ components) are capable of representing such systems, there is only one primary method for evaluating the reliability– through simulation. Furthermore, DPRA studies published in the literature tend to analyse systems, continuous dynamics of which are fully described within one or two physical domains, whereas such an analysis of multi-domain systems is largely unexplored.

Therefore, the development of dynamic reliability tools in general and application of such tools to PEMFCs are two attractive areas of research. Consequently, this paper has two objectives. First objective is to outline an approach to the development of an extended PEMFC model that satisfies the four fundamental requirements of dynamic reliability methods mentioned above. Second objective is to demonstrate how such a model can be used for dynamic reliability analysis.

### **3. Modelling Method**

The modelling approach proposed in this paper aims to rectify the limitations of classical reliability modelling techniques by considering the physical behaviour of the system together with possible events occurring during the system lifetime. In order to do this, two sub-models – deterministic and stochastic are developed and linked together to create an overall hybrid model. In the following sections, the deterministic sub-model is discussed first, followed by the stochastic one.

### **4. Deterministic Model**

The model is developed with the bond graph approach and is an extension of the model developed by Vasilyev et al. [36]. The original model contains a set of differential equations that describe the continuous time dynamics of state variables such as pressure, temperature and mass flows. Quantities such as membrane thickness were assumed constant. The model is implemented using object-oriented approach using physics-based modelling language Modelica.

In this work in order to take into account the ageing and degradation mechanisms previously static parameters related to the membrane electrode assembly are made dynamic. Time-evolution of these variables dictates the power output of the fuel cell system. Some of the most important equations are provided here, but more information can be found in various books and publications, for example [37]. In order to differentiate between the static and dynamic quantities the superscript <sup>†</sup> is used to mark the variables that are modified to incorporate degradation.

#### 4.1. Voltage Output

The maximum electrical potential of an ideal fuel cell at open circuit and given temperature and pressure is determined by the Nernst equation:

$$E_{Nernst} = -\frac{\Delta G}{2F} + \frac{RT}{2F} \ln \left( \frac{p_{H_2} \sqrt{p_{O_2}}}{p_{H_2O}} \right) \quad (3)$$

where  $\Delta G$  is the change of Gibbs free energy,  $F$  is the Faraday constant ( $96485 \text{ C/mol}$ ),  $R$  is the ideal gas constant ( $8.314 \text{ J mol}^{-1} \text{ K}^{-1}$ ),  $T$  is the temperature (K),  $p_{H_2}$ ,  $p_{O_2}$ ,  $p_{H_2O}$  are partial pressures of hydrogen, oxygen and water vapour (Pa). However, as soon as the electrical load is applied to the cell, different voltage loss mechanisms begin to occur. As a result the output voltage is expressed by the following equation:

$$U_{cell} = E_{Nernst} - \eta_{act} - \eta_{ohm} - \eta_{conc} \quad (4)$$

Where terms  $\eta_{act}$ ,  $\eta_{ohm}$ ,  $\eta_{conc}$  describe the voltage loss phenomena described in the following sections.

##### 4.1.1. Activation Losses and Catalyst Degradation

Activation losses  $\eta_{act}$  represent the amount of energy consumed to overcome the activation barrier and sustain the electrochemical reaction:

$$\eta_{act}^{\dagger} = \frac{RT}{\alpha F} \ln \left[ \frac{i + i_{loss}^{\dagger}}{i_0^{\dagger}} \right] \quad (5)$$

where  $i$  is the current density,  $i_{loss}$  describes the amount of current density loss due to the direct electron transfer through the membrane bypassing the external load and  $\alpha$  is the transfer coefficient. As the fuel cell ages the parameters  $i_{loss}$  and  $i_0$  change in value, the evolution of  $i_0$  is described below with  $i_{loss}$  considered in section 4.1.2. The exchange current density  $i_0$  is a characteristic of the reaction rate and it is a function of temperature, partial pressure of the reactants and catalyst layer properties [38]. For the cathode electrode  $i_0$  is given by Equation 6:

$$i_0^{\dagger} = i_0^{ref} \frac{A_{ec}}{A_{fc}} \left( \frac{p_{O_2}}{p_{O_2}^{ref}} \right)^{0.5} \exp \left[ -\frac{\Delta G^*}{RT} \left( 1 - \frac{T}{T^{ref}} \right) \right] \quad (6)$$

Where  $i_0^{ref} = 1 \times 10^{-9}$  [25] is the reference exchange current density,  $A_{ec}$  is the catalyst electrochemical surface area,  $A_{fc}$  is the nominal area of the PEMFC,  $p_{O_2}$  is the partial pressure of oxygen at the catalyst layer,  $p_{O_2}^{ref}$  and  $T^{ref}$  are reference pressure and temperature,  $\Delta G^* = 66 \text{ kJ mol}^{-1}$  is the activation energy of the oxygen reduction reaction at the cathode electrode.

It is known that over time the catalyst electrochemical surface area decreases due to a process during which smaller Pt- particles agglomerate into larger ones, thus reducing the total geometric area of the catalyst particles  $A_{geo}$  [3]. The geometric and electrochemical surface areas are proportional to each other with the coefficient of proportionality dependent on the MEA properties. Zhang and Pisu [39] estimated that  $A_{ec}/A_{geo} = 0.63$  and proposed a first-order ODE to describe the degradation of the catalyst geometric area as expressed in Equation 7:

$$\frac{dA_{geo}}{dt} = -\Phi_A \frac{4k_1}{9V_{Pt}^2} \frac{M_{Pt}}{\rho_{Pt}} \frac{F\alpha_1}{RT} \exp\left[\frac{F}{RT}\left(\Delta\phi_C - U_1^\theta + \frac{\alpha_1 A_{geo}}{V_{Pt}}\right)\right] A_{geo}^3 \alpha_r \beta_r^2 \quad (7)$$

where  $\Phi_A$  is a fitting parameter,  $k_1 = 1 \times 10^{-9} \text{ mol/cm}^2/\text{s}$  and  $U_1^\theta = 1.18 \text{ V}$  are the rate constant and the standard equilibrium potential of Pt dissolution reaction respectively,  $M_{Pt} = 195.1 \text{ g/mol}$  and  $\rho_{Pt} = 21.45 \text{ g/cm}^3$  are the molar mass and density of Pt respectively,  $\alpha_1 = 1.14 \times 10^{-10}$  is a constant parameter, parameters  $\alpha_r = 1.1$  and  $\beta_r = 0.038$  characterise the radius of the Pt-particle groups relative to the mean radius of the total particle population.  $\Delta\phi_C$  is the phase potential difference between the electrolyte phase and the cathode phase calculated using Equation 8:

$$\Delta\phi_C = U_{cell} + i \cdot A_{fc} \cdot R_{ohm} \quad (8)$$

The initial value of  $A_{geo}$  is calculated using Equation 9 assuming that each Pt is a perfect sphere.

$$A_{geo}^0 = 4\pi r_{Pt}^2 N_{Pt} \quad (9)$$

where  $r_{Pt}$  is the average radius of Pt-particles and  $N_{Pt}$  is the number of particles in the group. Similarly, the volume of the platinum catalyst is estimated using Equation 10:

$$V_{Pt} = \frac{4}{3}\pi r_{Pt}^3 N_{Pt} \quad (10)$$

#### 4.1.2. Ohmic Losses and Membrane Degradation

Ohmic losses  $\eta_{ohm}$  result from the fuel cell's internal resistance to the transport of charged particles (electrons and ions), i.e. ohmic  $R_{ohm}$  and ionic  $R_{ion}$  resistances:

$$\eta_{ohm} = I(R_{ion} + R_{ohm}) \quad (11)$$

where  $I$  is the current load. It is important to note that  $R_{ion}$  is a strong function of water content within the membrane.

Modelling membrane degradation is also limited to primarily using empirical or semi-empirical relations due to the complexity of interacting mechanisms and lack of experimental data. Nevertheless, Chandesris et al. [40] recently suggested the following equation to describe the mechanism of membrane thinning due to fluoride ( $F^-$ ) release:

$$v_{F^-} = \Phi_1 \frac{\Delta p_{O_2}}{p^{ref}} \frac{\delta_{mem}^0}{\delta_{mem}^\dagger} \exp \left[ \frac{\alpha_{eq} F}{RT} U_{cell} \right] \exp \left[ -\frac{\Delta G^{**}}{R} \left( \frac{1}{T} - \frac{1}{T^{ref}} \right) \right] \quad (12)$$

where  $v_{F^-}$  is the fluoride release rate,  $\Phi_1 = 1.7 \times 10^{-7}$   $\mu\text{g}/\text{cm}/\text{h}$  is a fitting parameter,  $p^{ref} = 101,325$  Pa is the reference pressure and  $\Delta p_{O_2} = p_{c,O_2} - p_{a,O_2}$  is the difference between partial pressures of  $O_2$  at cathode and anode sides. The initial and effective thickness of the membrane are denoted by  $\delta_{mem}^0$  and  $\delta_{mem}^\dagger$ ,  $\alpha_{eq} = 0.54$  is an equivalent transfer coefficient and  $\Delta G^{**} = 75 \text{ kJ mol}^{-1}$  is the activation energy of the chemical reactions causing degradation.

The change in membrane thickness is then expressed in terms of the fluoride release rate as follows:

$$\frac{d\delta_{mem}^\dagger}{dt} = -\Phi_2 \frac{v_{F^-}}{\omega_{F^-}} \rho_{mem} \quad (13)$$

Where  $\Phi_2=20.8$  is a fitting parameter,  $\omega_{F^-}=0.82$  is the fraction of fluoride within Nafion and  $\rho_{mem} = 0.00197 \text{ kg}/\text{cm}^3$  is the dry density of the membrane. Equation 12 shows that the fluoride release rate grows exponentially with increasing voltage, which means that when the fuel cell is at open circuit, the rate of membrane degradation is at its highest.

The reduction of membrane thickness results in an increase of crossover currents, since it shortens the diffusion path through the membrane. This leads to an increase in the crossover current density which can be calculated as:

$$i_{loss}^\dagger = \frac{p_{an} K_{H_2}}{\delta_{mem}^\dagger} 2F \quad (14)$$

Where  $K_{H_2} = 3.68 \times 10^{-16} \text{ mol Pa}^{-1} \text{ cm}^{-1} \text{ s}^{-1}$  is the permeability of  $H_2$  through the membrane and  $p_{an}$  is the total gas pressure in the anode volume.

Furthermore, the ageing of the membrane also results in the change of its ionic conductivity properties. The following exponential relation was suggested by Jouin et al. [41]:

$$R_{ion}^\dagger = R_{ion} \exp(\beta_{ion} t) \quad (15)$$

where  $R_{ion}$  is the value of membrane ionic resistance and  $\beta_{ion}$  is the membrane degradation parameter.

#### 4.1.3. Concentration Losses

The concentration overpotential  $\eta_{con}$  occurs at higher current densities when the reactants are consumed faster than they are supplied. Under such conditions, the concentration of fuel or oxidant at the catalyst layer tends to 0 leading to drastically reduced voltage output. The effects of  $O_2$  partial pressure at cathode side is the primary factor for the occurrence of the concentration losses which can be expressed as follows [25]:

$$\eta_{con}^\dagger = \frac{RT}{4\alpha F} \ln \left( \frac{i_L^\dagger}{i_L^\dagger - i} \right) \quad (16)$$

Where  $i_L$  is calculated using Equation 17:

$$i_L^\dagger = \frac{zF}{RT} \frac{D_{gas}^\dagger}{\delta_{GDL}} p_i \quad (17)$$

Changes in mass transport properties of the GDL due to degradation can be expressed through the changes of the diffusivity of gases within the diffusion medium as follows [41]:

$$D_{gas}^\dagger = D_{gas} + \beta_D t \quad (18)$$

where  $D_{gas}$  is the initial value of diffusivity of gases through the GDL and  $\beta_D$  is the degradation parameter.

Jouin et al. [41] also suggest incorporating the increase of concentration losses by modifying Equation 16 with a degradation parameter  $\beta_B$  as follows:

$$\eta_{con}^\dagger(t) = \left( \frac{RT}{4\alpha F} + \beta_B t \right) \ln \left( \frac{i_L^\dagger}{i_L^\dagger - i} \right) \quad (19)$$

Furthermore, the increase of internal ohmic resistance of the fuel cell was described by the following linear equation [41]:

$$R_{ohm}^\dagger = R_{ohm} + \beta_{ohm} t \quad (20)$$

where  $R_{ohm}$  is the initial value of internal resistance,  $\beta_{ohm}$  is the parameter describing the rate of degradation.

#### 4.2. Pressure dynamics

The ideal gas law determines the changes in reactant pressure within the volume of gas supply channels:

$$\frac{m_{gas} V_{ch}}{RT} \left( \frac{dP}{dt} \right) = \sum_{in/out} \dot{m}_{gas} \quad (21)$$

where  $P$  is the total pressure of the gases in the gas flow channels,  $V_{ch}$  is the volume of the channels and  $m_{gas}$  is the total mass of gases.

#### 4.3. Thermal dynamics

The temperature of the fuel cell changes according to the following energy balance equation:

$$c_p m_{fc} \frac{dT}{dt} = \dot{Q}_{fc} - \dot{Q}_{cool} \pm \dot{Q}_{amb} + \dot{H}_{in} - \dot{H}_{out} \quad (22)$$

where  $c_p$  is the specific heat capacity of the fuel cell,  $m_{fc}$  is the mass of the cell,  $\dot{Q}_{fc}$  is the amount of heat generated by the reaction,  $\dot{Q}_{cool}$  is the amount of thermal energy exchanged with the coolant,  $\dot{Q}_{amb}$  is the heat loss to the environment,  $\dot{H}_{in}$  and  $\dot{H}_{out}$  are the enthalpies of the gases carried in and out of the fuel cell stack calculated as follows:  $\dot{H}_{in/out} = c_{p,gas} \dot{m}_{gas} T_{gas}$ .

#### 4.4. Nitrogen Diffusion and Purging

The existing model is augmented with an additional mechanism of nitrogen ( $N_2$ ) diffusion through the membrane. This phenomenon becomes important when the fuel cell is operated under ‘dead-end’

configuration. Such a configuration means that the outlet of the anode side of the fuel cell is closed, thus ensuring the increased H<sub>2</sub> utilisation. However, as N<sub>2</sub> diffuses through the MEA, the partial pressure of H<sub>2</sub> drops. As a result, it becomes necessary to vent the N<sub>2</sub> from the anode by opening the outlet controlled by a dedicated purge valve. According to Chen et al [42], the N<sub>2</sub> flux,  $\dot{n}_{N_2}$  is given by:

$$\dot{n}_{N_2} = D_{N_2} \frac{p_{c,N_2} - p_{a,N_2}}{\delta_{mem}^\dagger} \quad (23)$$

Where  $p_{c,N_2}$  and  $p_{a,N_2}$  are N<sub>2</sub> partial pressure on the cathode and anode sides of the membrane and  $D_{N_2}$  is the diffusion coefficient of N<sub>2</sub> through the membrane and can be calculated from [43]:

$$D_{N_2} = \frac{k_{N_2} p_{c,N_2}}{C_{N_2}} \quad (24)$$

Where  $C_{N_2}$  is the N<sub>2</sub> concentration in the cathode volume and  $k_{N_2}$  is the nitrogen permeability coefficient within the membrane. Calculated according to Equation 25 [44]:

$$k_{N_2}(T_{cell}) = \Phi_{N_2} (0.0295 + 1.21f_v - 1.93f_v^2) \times 10^{-14} \times \exp\left[\frac{\Delta G_{N_2}}{R} \left(\frac{1}{T_{ref}} - \frac{1}{T_{cell}}\right)\right] \quad (25)$$

where  $\Phi_{N_2}$  is an empirical parameter to be identified from experiments,  $\Delta G_{N_2} = 24$  kJ/mol,  $T_{ref} = 303$  K and  $f_v$  is the volume fraction of water inside the membrane.

#### 4.5. Parameter Estimation

The equations in Sections 4.1-4.4 contain several empirical parameters, values of which need to be identified from experimental observations or from the literature. The degradation coefficients in the equations can be identified from publicly available ageing data obtained from a 5-cell stack with 100cm<sup>2</sup> active area over 1150 h of operation under constant conditions [45]. During the experiment the current load was set to 70 A, stack temperature maintained around 55 °C with a steady coolant flow of 2 L/min while anode and cathode pressures were also maintained constant at about 1.3 bar. The data was analysed to estimate the parameter values which are given in Table 1.

Table 1: Estimated parameter values for the 5-cell stack.

Symbol	Value	Units
$\alpha$	0.55	-
$R_{ohm}$	0.41	$\Omega/\text{cm}^2$
$N_{Pt}$	$2.24 \times 10^{16}$	-
$A_{geo}^0$	19005	$\text{cm}^2$
$V_{Pt}$	$1.6 \times 10^{-3}$	$\text{cm}^3$
$\Phi_A$	$2.5 \times 10^6$	-

$\beta_R$	$3.127 \times 10^{-9}$	$\Omega/\text{hr}$
$\beta_{ion}$	$2.058 \times 10^{-8}$	$\text{hr}^{-1}$
$\beta_B$	$2.57 \times 10^{-5}$	$\text{V}/\text{hr}$
$\beta_D$	$1 \times 10^{-6}$	$\text{cm}^2/(\text{s} \times \text{hr})$

Using the parameters listed in Table 1 the simulated voltage fits the experimental data exceptionally well with mean absolute error being only  $8 \times 10^{-3}$  V, and mean relative error of 0.25% as shown in Figure 2.

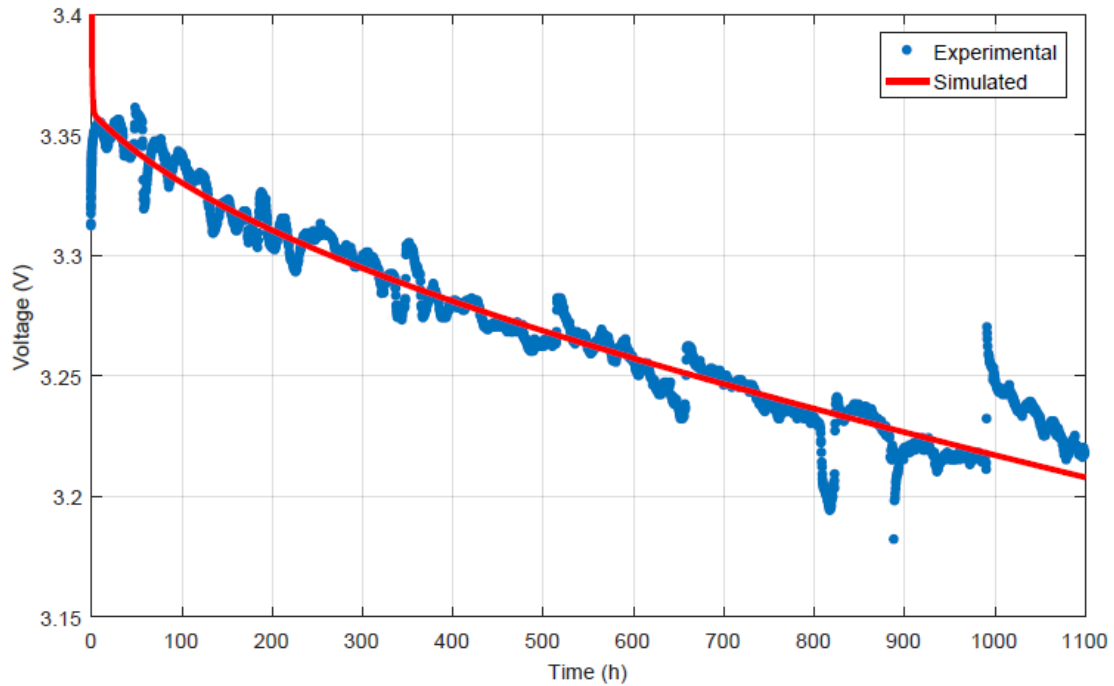


Figure 2. Experimental and fitted voltage degradation over 1100 hours

## 5 Stochastic Model

The stochastic sub-model is dedicated to modelling failures of the supporting components within the fuel cell system. This part of the hybrid model operates in discrete-time domain and it is implemented with Stochastic Petri nets (SPNs) making it capable of representing different component states and events occurring during a fuel cell lifetime.

Petri nets are a graphical and mathematical modelling tool for representation of a variety of systems and processes. A Petri net is a bipartite graph consisting of two types of nodes – places and transitions. A collection of places represents the set of possible system states. Transitions between the places correspond to various events that occur during the system lifetime. Tokens move between places via the

transitions and the state of the system at any point in time is characterised by the marking of the Petri net by the tokens. The transitions fire when certain conditions are met. In the model developed here all transitions are timed and hence a delay is associated with all transitions once the condition for firing are met. For timed transitions the delay can be determined randomly or be predetermined intervals of time. Graphically, places are represented by circles and transitions are drawn as rectangles.

Many software tools exist for creating and simulating PNs, but since the deterministic sub-model was developed using the Modelica language, it is natural to use a PN library within this modelling environment. So a library called PNlib developed by Proß & Bachmann [47] was applied for modelling the stochastic sub-model. This is an open-source library that contains the code and graphical representation for all essential Petri net elements. Figure 3 shows nets developed using PNlib for a component with (a) one failure mode and (b) two failure modes. A place marked with an integer  $k$  is said to contain  $k$  tokens. In (a) the two states  $C1\_W$  and  $C1\_FM1$  represent the working and failed states of a generic component  $C1$ . When the place  $C1\_W$  contains a token, as it does in Figure 3(a), then the transition  $T1$  is said to be enabled and will fire after the delay associated with it. The delay in this example would be the time to failure of the component  $C1$ . When transition  $T1$  fires it moves the token from  $C1\_W$  to  $C1\_FM$  thus representing a failure event. In (b) there are three states  $C2\_W$ ,  $C2\_FM1$  and  $C2\_FM2$  representing component  $C2$  working,  $C2$  failed in failure mode 1 and  $C2$  failed in failure mode 2 respectively. There is a token in the place  $C2\_W$  meaning that both transition  $T2$  and  $T3$  are enabled. The transition with the shortest delay will fire and the token marking state  $C2\_W$  will be moved to the state corresponding to the respective failure mode ( $C2\_FM1$  or  $C2\_FM2$ ). Additional failure modes can be added in a similar fashion.

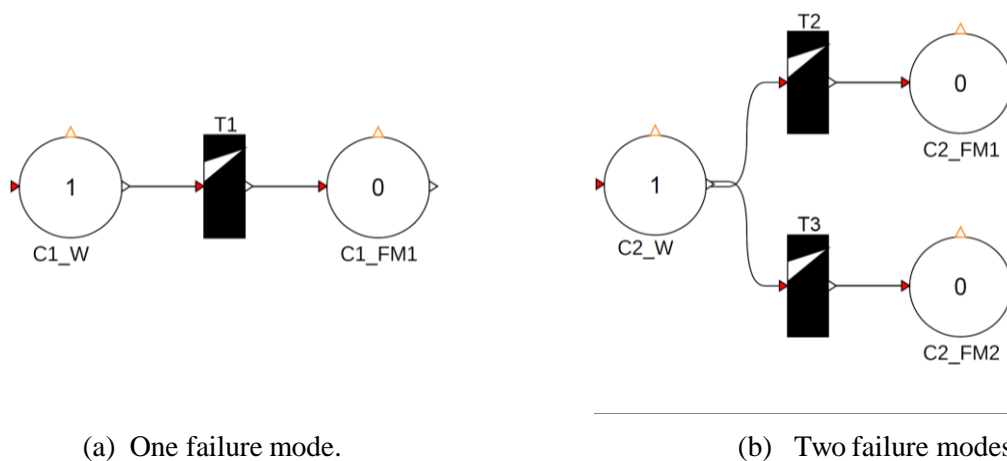


Figure 3. Petri Net representation of component failure modes using PNlib in Modelica.

Individual PN's like those shown in Figure 3 have been implemented for each failure mode of each auxiliary component in the PEMFC system. In order to determine the delays associated with the transitions the times to failure for the components needs to be determined. In order to do this the

probability of occurrence of each failure mode is modelled by a 2-parameter Weibull distribution. This distribution is one of the most commonly used in reliability engineering due its flexibility to fit many other probability distributions [48]. In this case, the probability of component failure at any instance in time can be characterised by an *unreliability function*  $F(t)$  which is given by:

$$F(t) = 1 - \exp \left[ - \left( \frac{t}{\eta} \right)^\beta \right] \quad (26)$$

where  $\beta$  is the shape parameter and  $\eta$  is the scale parameter. The transition firing intervals for each failure model  $t_{fire}$  can be obtained by taking the logs of both sides of equation (26) and rearranging to give:

$$t_{fire} = \eta [-\ln(1 - F(t))]^{1/\beta} \quad (27)$$

Where  $F(t)$  takes values in the interval [0,1].

The auxiliary components considered in this work are based on the PEMFC system defined in [4]. Table 2 contains the list of components grouped by the corresponding sub-system and their respective failure modes. The values of parameters  $\beta$  and  $\eta$  are gathered from the literature [49; 50] and listed in Table 2 along with the corresponding failure modes for the components. It is important to note that  $\beta = 1$  for all the failure modes due to the fact that the reliability data is usually gathered under the assumption of constant failure rate. This assumption is justified if early life failures are eliminated by extensive testing before installation, while end-of-life failures are also eliminated because a component is assumed to be replaced before it reaches that point in its lifetime.

Table 2: Component failure modes and the corresponding Weibull parameters.

Sub-system	Component	Failure Mode	$\beta$	$\eta, 10^6$ h	Source
Fuel supply	H <sub>2</sub> solenoid valve	Fails to function	1	0.2	[38]
	H <sub>2</sub> supply line	Leak or rupture	1	1	[38]
Fuel processing	Low-pressure H <sub>2</sub> filter	Restrict or limit flow	1	1	[38]
		Hole in filter media	1	1	[38]
	H <sub>2</sub> humidifier	Fails to function	1	0.004	[38]
		Leak or rupture	1	0.004	[38]
		Leak or rupture	1	0.01	[38]
Air supply	Air blower	Fails to function	1	0.04	[38]
	Air compressor	Fails to function	1	0.008	[38]
	Air flow meter	Fails to function	1	0.05	[38]
	Air line	Leak or rupture	1	1	[38]
Air processing	Air filter	Restrict or limit flow	1	1	[38]

		Hole in filter media	1	1	[38]
	Air humidifier	Fails to function	1	0.004	[38]
		Leak or rupture	1	0.004	[38]
Thermal Management	Radiator	Restrict or limit flow	1		[38]
		Fails to function	1		[38]
	Coolant pump	Fails to function	1	0.01	[37]
		Leak or rupture	1	0.01	[38]
	Coolant line	Leak or rupture	1	1	[38]

In order to integrate the stochastic and deterministic models, failures of the auxiliary components in the stochastic model need to be converted into disturbances to the process variables in the deterministic model. In the stochastic model the times to failure of the components are generated using equation (27), this defines the transition times in the PN modules and determines the placement of tokens in the models. Once a token resides in a component failure place, such as C1\_FM1 in figure 3(a), the Modelica Standard Library is used to generate a failure signal which is passed to the deterministic model where the relevant process variables are altered.

This is illustrated in Figure 4 which depicts a section of the resulting hybrid model. The lower part of Figure 4 represents the fuel supply sub-system, where the ‘Gas mix’ block determines the molar gas composition of the fuel; block ‘mSe’ represents the pressure source; block ‘Rth’ corresponds to a valve and the two thick arrows with letter ‘N’ indicate the direction of gas flow (for a more detailed description of each of these blocks see [36]). The upper part of Figure 4 contains a PN module representing a single failure mode of the valve with transition T1 and two places P1 and P2. The state of the component is interpreted from the presence or absence of token within P2 through blocks integerToBoolean and TriggeredTrapezoid, which generates the fault signal F(t). This signal serves as an input to a valve represented by bond-graphic block Rth and increases the valve resistance and consequently reducing its throughput. All other components listed in Table 2 are connected to the corresponding PN modules in the same fashion.

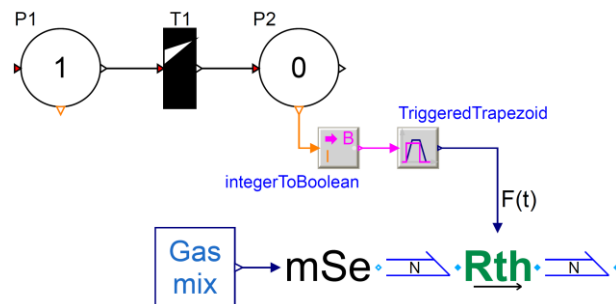


Figure 4. Arrangement of blocks to translate the state of Petri net into the dynamic variables of the fuel

supply sub-system of the overall physics-based model.

## 6 Monte Carlo Simulations

Simulation-based reliability analysis relies on the method called Monte Carlo simulation, which is often used when the model contains a high degree of uncertainty in its parameters and provides the means to analyse a wide number of possible scenarios of system life-time evolution. The method consists of iteratively generating a set of random input parameters, then using them to evaluate the deterministic model and recording the outputs. After completing a large number of simulations, statistical information about the system performance and its reliability characteristics can be gathered and assessed.

### 6.1 Parameter Uncertainty

The values of parameters  $\beta_{ohm}$ ,  $\beta_{ion}$ ,  $\beta_B$ ,  $\beta_D$  and  $\Phi_A$  listed in Table 1 are highly uncertain and strictly speaking cannot be used when attempting to simulate the behaviour of a different fuel cell stack even under similar operational conditions. The uncertainty comes from many sources such as natural unit-to-unit variability occurring during component manufacturing, assembly and operation. Furthermore, the values of these parameters often cannot be directly measured. Therefore, in order to account for the uncertainty in estimation, values of these parameters can be obtained from a set of random statistical distributions. Many types of such distributions exist, such as the already mentioned Weibull, exponential, uniform, normal and many others. Each of the distributions has a unique set of properties and can be used in various applications. The choice of a particular distribution can be guided by the experimental measurements, but when the data is scarce, an estimated distribution can be assumed. Nogue et al. [51] distinguished three types of parameter uncertainty: optimistic (normal distribution), pessimistic (uniform distribution) and realistic (Weibull distribution). It is impossible to infer the parameter uncertainty distribution from just one lifetime worth of measurements, so a guessed distribution is suggested.

From Equations 15 and 18 to 20, it can be inferred that the values of the degradation parameters  $\beta_{ohm}$ ,  $\beta_{ion}$ ,  $\beta_B$  and  $\beta_D$  should be located on the semi-infinite interval  $[0, \infty)$ . The shape of the distribution can be assumed to be normal with the mean around the values in Table 1 and standard deviation of 25% of the mean. However, the normal distribution is defined on the range  $(-\infty, \infty)$ , but it can be truncated at 0 to obtain a truncated normal distribution defined on  $[0, \infty)$ . Table 3 lists the parameters with associated distribution types and their suggested characteristic properties.

Table 3: Degradation distributions characteristics.

Parameter	Distribution	Interval	Estimated	Suggested
			$\mu$	$\sigma$

$\Phi_A$	Normal	$(-\infty, \infty)$	$25 \times 10^5$	$25 \times 10^4$
$\beta_{ohm}$	Truncated normal	$[0, \infty)$	$5 \times 10^{-5}$	$1.6 \times 10^{-5}$
$\beta_{ion}$	Truncated normal	$[0, \infty)$	$5 \times 10^{-5}$	$1.6 \times 10^{-5}$
$\beta_B$	Truncated normal	$[0, \infty)$	$1 \times 10^{-6}$	$1.6 \times 10^{-5}$
$\beta_D$	Truncated normal	$[0, \infty)$	$1 \times 10^{-6}$	$1 \times 10^{-5}$

---

It is reasonable to suggest that the parameter uncertainty distributions may have different characteristics or shape for different operating regimes. For example, for steady-state operation, the standard deviation of a parameter may be smaller, while during dynamic operation, it can increase. However, additional empirical data for a variety of operating modes is needed to make an informed decision about this. Consequently, in this paper it is assumed that the distribution type remains the same for each operating mode and the standard deviation values in Table 3 are large enough to cover all operating modes.

## 6.2. Simulation Design

The durability target for the fuel cell system is 5000 h with 10 % loss of performance. Therefore, the simulations are set to run until 5000 h is reached and are stopped prematurely either when the degradation threshold of 10 % is reached or a failure of any of the supporting components occurs. In order to see how changes of operating conditions affect the system reliability, two scenarios are investigated. In the first scenario a constant current load of 70 A was applied to the fuel cell and the rest of the operating conditions were set to be the same as those in the dataset used to identify the model parameters. In the second scenario, a dynamically changing current profile corresponding to the New European Drive Cycle (NEDC) was applied. The current variations span a range of values between 0 and 100 A and are depicted in Figure 5.

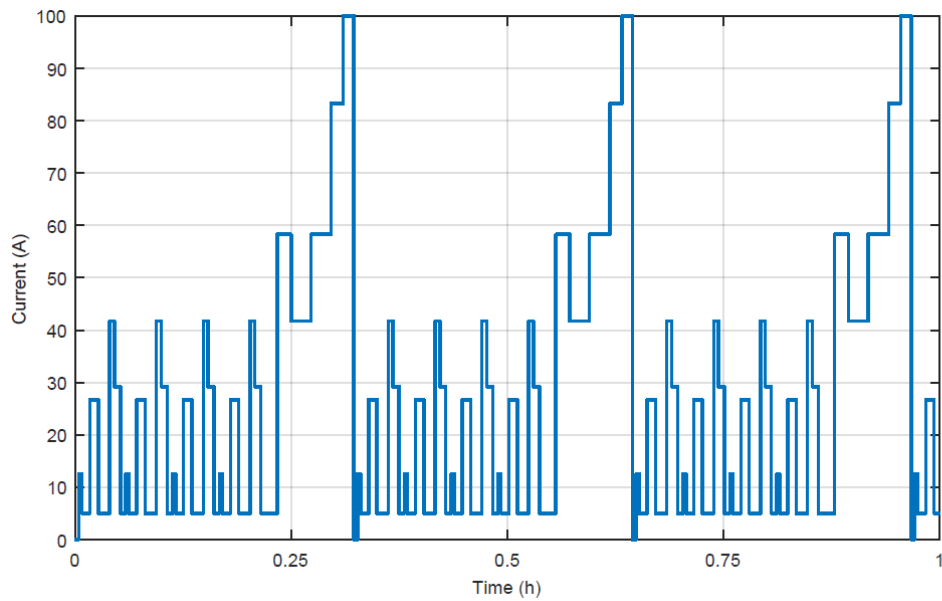


Figure 5: New European Drive Cycle profile applied to the fuel cell.

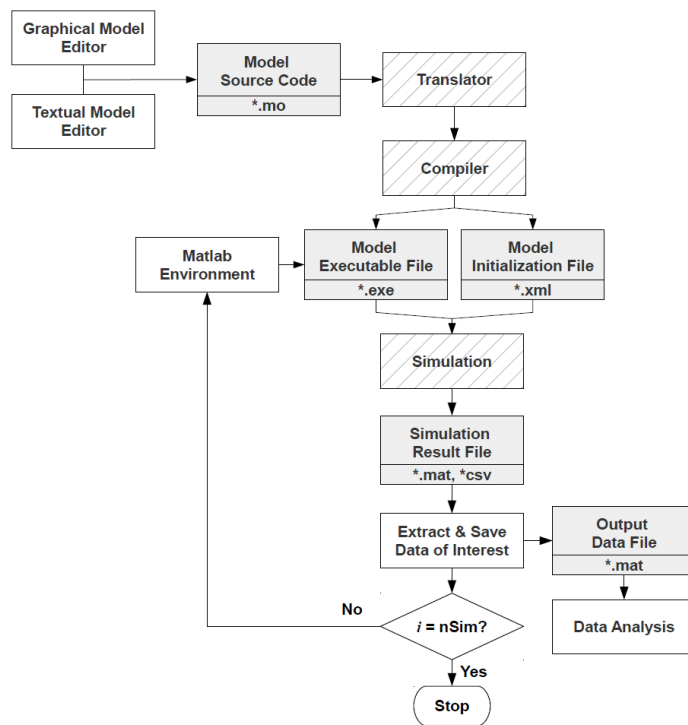


Figure 6: Monte Carlo simulation flow-chart.

The Monte Carlo simulation is set-up using the Matlab environment and the process logic is illustrated in Figure 6. Matlab repeatedly calls the model executable file for a set number of simulations,  $n_{sim}$ . After an individual simulation is complete, the necessary information such as the calculated stack voltage and the failure modes are extracted from the result file and stored in an output file for future analysis. This process is repeated until the total number of simulations is completed. There is no single way of selecting the total required number of Monte Carlo iterations since the output

depends on the desired accuracy and the variance of parameters within the model [48]. In order to identify the stopping point, it was decided to monitor how the mean survival time of the system was changing with every iteration and stop the execution when a desired degree of convergence is reached. The resulting graph for the first scenario is depicted in Figure 7 (the graph is very similar for the second scenario and thus not shown here), which shows that after the initial oscillations during the first 200 iterations, the mean survival time converged at approximately 2470 h. Therefore, it is sufficient to stop the algorithm execution when such convergence is reached. However, because the model contains different sub-systems, it is beneficial to perform a larger number of simulations in order to obtain a more detailed insight into the different failure modes of the system. Because of this, the Monte Carlo algorithm was stopped after 500 iterations were completed and the data was processed.

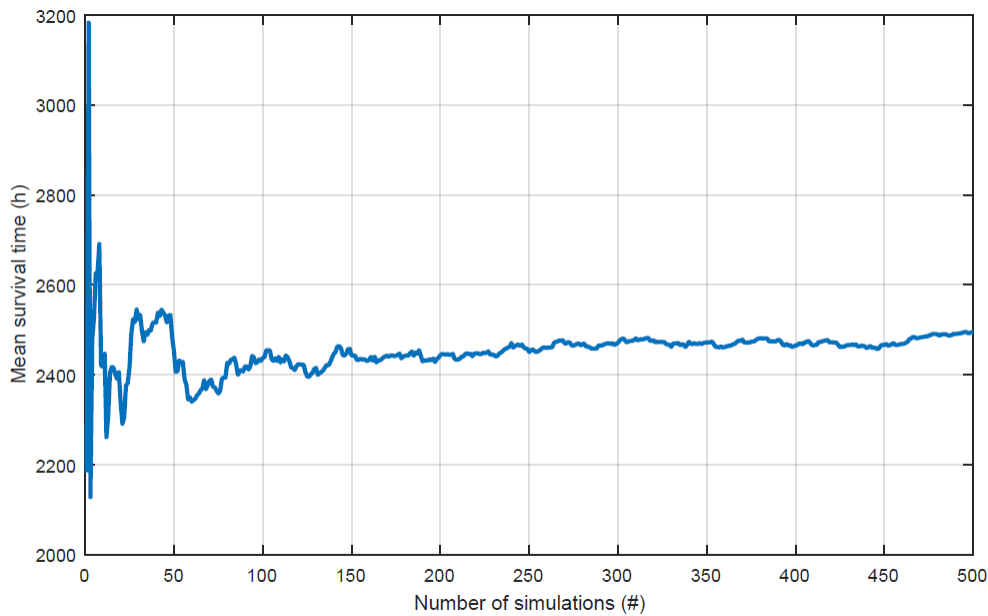


Figure 7: Mean survival time versus the number of Monte Carlo runs.

## 7 Simulation Results

After the defined number of simulations is complete, the collected data is sorted and expressed as shown in Table 4. Each simulation run constitutes an individual observation. The first column contains the observation numbers, the entries in the second column signify whether the fuel cell system failed (F) or survived until the cut-off point of 5000 h and was suspended (S). Since the failure times of the suspended runs are unknown, these values are censored and not included in the analysis. The last column in this table signifies the corresponding system failure mode as denoted by the sub-system name or labelled as 'unknown' if an observation was suspended.

Table 4: Table of times to failure.

Observation number	State	Failure time (hr)	Failure mode
--------------------	-------	-------------------	--------------

1	F	1395	Thermal management
2	F	2487	Fuel supply
3	F	1693	Stack
4	S	5000	Unknown
...	...	...	...
500	F	3152	Air supply

The collected lifetime data was analysed for the scenarios considered. Figure 8 shows a histogram of the times to failure for the case when a constant current load of 70 A was applied to the fuel cell.

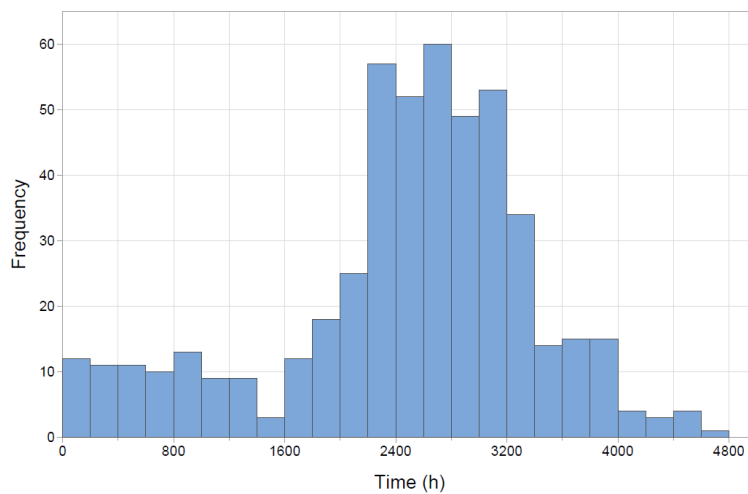


Figure 8. Histogram of system times to failure under constant 70A load.

This histogram reveals a pattern for failure occurrences of the system. It can be seen that although there are some early-life failures (up to 1600 h to 1800 h), the majority of failures take place between approximately 2000 h and 3400 h. After 3400 h the frequency decreases and falls off to almost 0 by 5000 h. Similarly, histograms for scenarios 2 and 3 are shown in Figures 9 and 10.

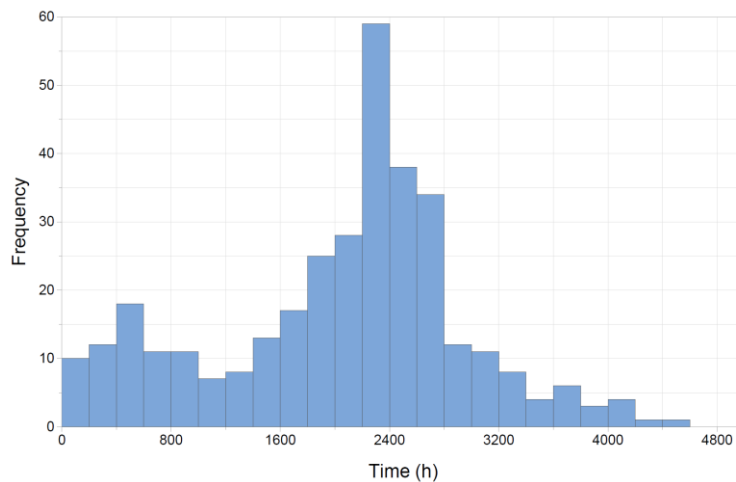


Figure 9. Histogram of system times to failure under dynamic NEDC load.

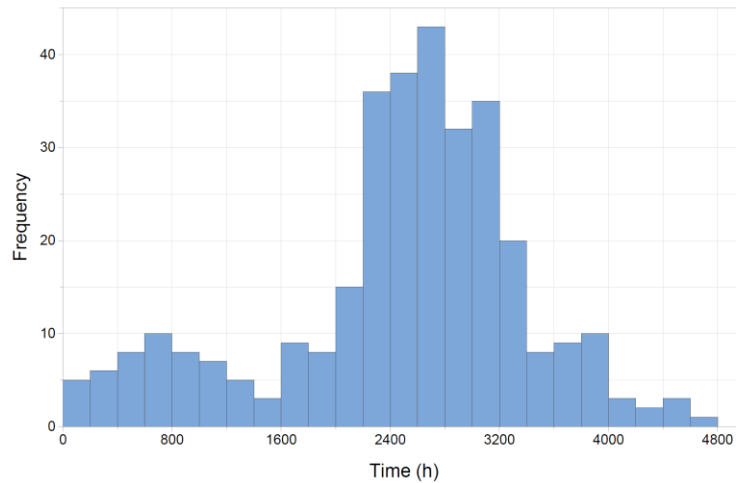


Figure 10. Histogram of system times to failure under constant 70 A load, but with anode purging (dead-end anode).

Histograms in Figures 8, 9 and 10 can significantly differ from each other visually depending on the column width, thereby making it difficult to compare the results. A more comprehensive way of analysing the data is by plotting an empirical Cumulative Distribution Function (eCDF). This provides a normalised overview of the survival data by calculating the cumulative sum of all the columns in the histogram and expressing it as a proportional value between 0 and 1. Figure 11 shows the calculated eCDF's for the three scenarios considered.

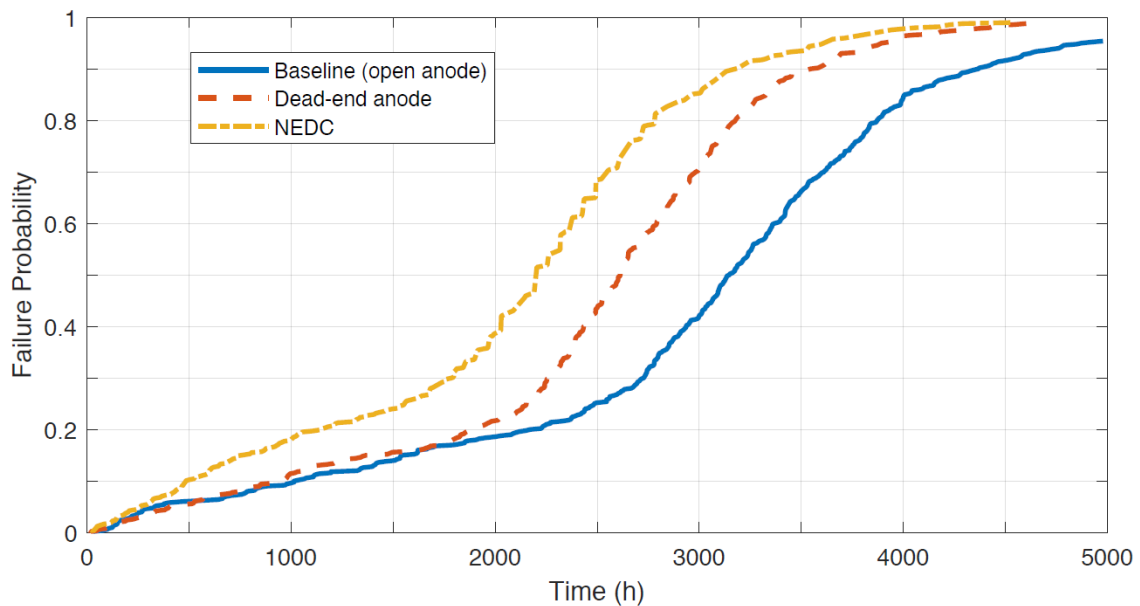


Figure 11. Empirical CDFs for different scenarios.

Also shown are values for the scenario when the fuel cell is operating in the ‘dead-end’ configuration. By observing the baseline eCDF, it can be seen that the probability of system failure by 2000 h is approximately 19%, but by 4000 h the probability soars to 84%. Only 5% of the population survive to 5000 h. The mean and median survival times for this case are 2978.69 h and 3147 h respectively. It is believed that the change in the slope of the eCDF after 2000 h is due to the occurrence of two different failure modes within the stack.

The eCDF calculated for the dynamic (NEDC) current load scenario yields a worse reliability performance than at constant load. At 2000 h, the probability of failure is 40 % and at 4000 h it reaches 97 %. The mean and median survival times for this case are 2083.84 h and 2204 h respectively. Such poor survivability of the system compared to the baseline is explained by the fact that the stack is operating in very intensive conditions, with large voltage variations constantly occurring as a result of repeating NEDC cycles.

The purging scenario also shows worse reliability characteristics than the base scenario. The mean and median survival times for this case are 2494.09 h and 2613 h respectively. An apparent increase in the failure probability can be seen after 2000 h, while unreliability in the early life remains almost the same as the baseline case. This observation is explained by the fact that each purging event subjects the membrane to additional mechanical stress caused by the periodic and abrupt pressure variations, thereby contributing to membrane degradation and failures.

To sum up, system reliability is shown to be low for all three cases, exhibiting the worst-case scenario of system lifetime. Probability of baseline scenario survival at the target time of 5000 h was found to be 5%, while the other two cases exhibit even lower probability. This is due to harsh operating conditions imposed on the stack. In reality, the stack will not be subjected to constant loads for extended periods of time. Likewise, dynamic loads in real vehicles occur only when driving.

The difference between reliability characteristics of the three investigated scenarios displayed in Figure 11, demonstrates the capability of the proposed model to calculate the dynamic reliability characteristics of PEMFC systems under varying operating conditions and control strategies.

Since the model was developed using open-source libraries and software, potential alterations can easily be implemented without requiring third-party licenses and tools. The model can be further extended to take into account daily and seasonal variations of ambient air temperature and humidity in different geographical locations. Using the model, a system designer can change the hardware configuration and set the corresponding reliability characteristics of the auxiliary components, define a different duty cycle (for example defined by automotive drive profiles such as WLTP, US06, etc.) and specify the climatic conditions. Performing another set of MC simulations using reconfigured model will yield a new dynamic reliability characteristic specific to the given model configuration and use case. Comparing the obtained dynamic reliability metrics for different system configurations can guide improvements in hardware design, control and maintenance strategy optimisation, as well as help with defining a more informed warranty policy. The ability to perform such analysis is a significant advantage over classical reliability methods, which cannot easily take into account variations in system operation during its lifetime.

## 8 Conclusions

In this paper, a novel modelling approach for reliability assessment of PEM fuel cells was presented. The approach expands the continuous-time deterministic dynamics of the system with discrete-time stochastic behaviour. The deterministic model was obtained by extending the model developed by Vasilyev et al. [36] to account for degradation and natural aging of the fuel cell. As failures of auxiliary components can lead to the disruption of conditions within the fuel cell and exacerbate degradation the failure of these components was modelled using Petri Nets and integrated with the deterministic model. The simulation of the resulting model enables dynamic reliability analysis of a fuel cell system to be performed. In this paper different Monte Carlo simulation scenarios were designed to observe the effects of changing operating conditions on the reliability of the system. The results show the clear influence of both purging and load cycles on the lifetime of a PEMFC system. Such results can be used to define a more robust maintenance strategy, assist with hardware design while achieving both improvements in performance and reliability.

The dynamic reliability analysis demonstrated in this paper can be further improved by incorporating dynamic ambient conditions, thereby demonstrating the effect of seasonal variations on the reliability of the system. Furthermore, performing MC simulations with more realistic load-cycles applied to the FC system will provide a more realistic lifetime prediction. Additional empirical data can be used for improved parameter estimation, making component degradation rates more accurate. Expanding on the Petri net aspect of the model provides an excellent opportunity to incorporate a more sophisticated system representation. For example, as well as modelling component failures can be expanded to include various maintenance schedules and spare parts availability.

## 9 Acknowledgements

The authors gratefully acknowledge the support of EPSRC (grant number EP/K02101X/1) which has enabled the research reported in this paper.

## 10 References

- [1] BP Statistical Review of World Energy, 2019, 68<sup>th</sup> edition, <https://www.bp.com/content/dam/bp/business-sites/en/global/corporate/pdfs/energy-economics/statistical-review/bp-stats-review-2019-full-report.pdf>
- [2] United Nations Framework Convention on Climate Change (UNFCCC), Paris Agreement (2020). [http://unfccc.int/paris\\_{\\_}agreement/items/9485.php](http://unfccc.int/paris_{_}agreement/items/9485.php)
- [3] H. Wang, H. Li, X.-Z. Yuan, PEM Fuel Cell Failure Mode Analysis, CRC Press, 2011.
- [4] US Department of Transportation, Failure Modes and Effects Analysis for Hydrogen Fuel Cell Vehicles – Subtask 1, Tech. Rep. February 2009.
- [5] N. Yousfi Steiner, D. Hissel, P. Moçotéguy, D. Candusso, D. Marra, C. Pianese, M.

- Sorrentino, Application of Fault Tree Analysis to Fuel Cell diagnosis, *Fuel Cells* 12, 2012, pp302-309.
- [6] L. Placca, R. Kouta, Fault tree analysis for PEM fuel cell degradation process modelling, *International Journal of Hydrogen Energy* 36 (19), 2011, pp12393–12405. doi:10.1016/j.ijhydene.2011.06.093.
- [7] S. Collong, R. Kouta, Fault tree analysis of proton exchange membrane fuel cell system safety, *International Journal of Hydrogen Energy* 40 (25), 2015, pp8248–8260. doi:10.1016/j.ijhydene.2015.04.101.
- [8] K. Brik, F. Ben Ammar, A. Djerdir, A. Miraoui, Causal and Fault Trees Analysis of Proton Exchange Membrane Fuel Cell Degradation, *Journal of Fuel Cell Science and Technology* 12 (5), 2015, doi:10.1115/1.4031584.
- [9] P. Rama, R. Chen, J. Andrews, Failure analysis of polymer electrolyte fuel cells., in: *Society of Automotive Engineers, [Special Publication] SP, Vol. SP-2167*, 2008, 109–125.
- [10] M. Whiteley, S. Dunnett, L. Jackson, Failure Mode and Effect Analysis, and Fault Tree Analysis of Polymer Electrolyte Membrane Fuel Cells, *International Journal of Hydrogen Energy* 41 (2), 2015, pp1187–1202. doi: 10.1016/j.ijhydene.2015.11.007.
- [11] British Standard, BS EN 62551:2012 Analysis Techniques for Dependability – Petri Net Techniques, 2012.
- [12] C. Wieland, O. Schmid, M. Meiler, A. Wachtel, D. Linsler, Reliability computing of polymer-electrolyte-membrane fuel cell stacks through Petri nets, *Journal of Power Sources* 190 (1), 2009, pp34–39. doi:10.1016/j.jpowsour.2008.10.010.
- [13] M. Whiteley, A. Fly, J. Leigh, S. Dunnett, L. Jackson, Advanced reliability analysis of Polymer Electrolyte Membrane Fuel Cells using Petri-Net analysis and fuel cell modelling techniques, *International Journal of Hydrogen Energy* 40 (35), 2015, pp11550–11558. doi:10.1016/j.ijhydene.2015.01.154.
- [14] Zhou, D., Pan, E., Zhang, X., & Zhang, Y. (2020). Dynamic Model-based Saddle-point Approximation for Reliability and Reliability-based Sensitivity Analysis. *Reliability Engineering and System Safety*, 201(February), 106972. <https://doi.org/10.1016/j.ress.2020.106972>
- [15] Zhang, Y., & Gu, J. (2020). Dynamic reliability analysis of angular contact ball bearings in positioning precision. *Proceedings of the Institution of Mechanical Engineers, Part O: Journal of Risk and Reliability*, 234(6), 723–734. <https://doi.org/10.1177/1748006X20933506>
- [16] Chiacchio, F., Aizpurua, J. I., Compagno, L., & D’Urso, D. (2020). SHyFTOO, an object-oriented Monte Carlo simulation library for the modeling of Stochastic Hybrid Fault Tree Automaton. *Expert Systems with Applications*, 146, 113139. <https://doi.org/10.1016/j.eswa.2019.113139>
- [17] M. Marseguerra, E. Zio, J. Devooght, P. Labeau, A concept paper on dynamic reliability via Monte Carlo simulation, *Mathematics and Computers in Simulation* 47, 1998, pp371–382. doi:10.1016/S0378-4754(98) 00112-8.

- [18] P. Labeau, C. Smidts, S. Swaminathan, Dynamic reliability: towards an integrated platform for probabilistic risk assessment, *Reliability Engineering & System Safety* 68 (3), 2000, pp219–254. doi:10.1016/S0951-8320(00)00017-X.
- [19] M. H. Davis, Piecewise-Deterministic Markov Processes: A General Class of Non-Diffusion Stochastic Models, *Journal of the Royal Statistical Society* 46 (3), 1984, pp353–388.
- [20] Schallert, C. (2011). Inclusion of Reliability and Safety Analysis Methods in Modelica (pp. 616–627). <https://doi.org/10.3384/ecp11063616>
- [21] Chiacchio, F., Aizpurua, J. I., Compagno, L., Khodayee, S. M., & D’Urso, D. (2019). Modelling and resolution of dynamic reliability problems by the coupling of simulink and the stochastic hybrid fault tree object oriented (SHyFTOO) library. *Information (Switzerland)*, 10(9). <https://doi.org/10.3390/info10090283>
- [22] Desgeorges, L., Piriou, P. Y., Lemattre, T., & Chraïbi, H. (2021). Formalism and semantics of PyCATSHOO: A simulator of distributed stochastic hybrid automata. *Reliability Engineering and System Safety*, 208(November 2020), 107384. <https://doi.org/10.1016/j.res.2020.107384>
- [23] M. Bouissou, H. Elmqvist, M. Otter, A. Benveniste, R. Edf, G. D. Gaulle, E. C. Paris, G. Voie, C. Malabry, Efficient Monte Carlo Simulation of Stochastic Hybrid Systems, in: 10th International Modelica Conference, Lund, Sweden, 2014, pp. 715–725. doi:10.3384/ECP14096715.
- [24] Lin, Y. H., Li, Y. F., & Zio, E. (2018). A comparison between Monte Carlo simulation and finite-volume scheme for reliability assessment of multi-state physics systems. *Reliability Engineering and System Safety*, 174(February), 1–11. <https://doi.org/10.1016/j.res.2018.01.008>
- [25] Shukla, D. K., & John Arul, A. (2020). A Review of Recent Dynamic Reliability Analysis Methods and a Proposal for a Smart Component Methodology. In P. V Varde, R. V Prakash, & G. Vinod (Eds.), *Reliability, Safety and Hazard Assessment for Risk-Based Technologies* (pp. 267–291). Singapore: Springer Singapore.
- [26] Taleb-Berrouane, M., Khan, F., & Amyotte, P. (2020). Bayesian Stochastic Petri Nets (BSPN) - A new modelling tool for dynamic safety and reliability analysis. *Reliability Engineering and System Safety*, 193(July 2019), 106587. <https://doi.org/10.1016/j.res.2019.106587>
- [27] D. Codetta-Raiteri, A. Bobbio, Evaluation of a benchmark on dynamic reliability via Fluid Stochastic Petri Nets, in: Proceedings of the 7th international workshop on performability modeling of computer and communication systems, 2005, pp. 52-55.
- [28] D. Codetta-Raiteri, A. Bobbio, Solving dynamic reliability problems by means of ordinary and Fluid Stochastic Petri Nets, *Advances in Safety and Reliability - Proceedings of the European Safety and Reliability Conference, ESREL 2005*.
- [29] G. Manno, A. Zymaris, N. Kakalis, F. Chiacchio, F. Cipollone, L. Compagno, D. D’Urso, N. Trapani, Dynamic reliability analysis of three non- linear aging components with different failure modes characteristics, in: *Safety, Reliability and Risk Analysis: Beyond the Horizon*, 2013, pp. 3047–3055.
- [30] F. Chiacchio, D. D’Urso, G. Manno, L. Compagno, Stochastic hybrid automaton model of a multi-state system with aging: Reliability assessment and design consequences, *Reliability*

Engineering & System Safety 149, 2016, pp1–13. doi:10.1016/j.ress.2015.12.007.

- [31] Rychkov, V., & Chraibi, H. (2017). Dynamic probabilistic risk assessment at a design stage for a sodium fast reactor. In *FR17: International Conference on Fast Reactors and Related Fuel Cycles: Next Generation Nuclear Systems for Sustainable Development* (pp. 1–8).
- [32] Shukla, D. K., & Arul, A. J. (2019). A smart component methodology for reliability analysis of dynamic systems. *Annals of Nuclear Energy*, 133, 863–880. <https://doi.org/10.1016/j.anucene.2019.07.027>
- [33] C. Schallert, Incorporation of Reliability Analysis Methods with Modelica, Proceedings of the 6<sup>th</sup> International Modelica Conference, 2008, pp. 103-112.
- [34] Shukla, D. K., & Arul, A. J. (2020). Static and dynamic reliability studies of a fast reactor shutdown system using smart component method. *Annals of Nuclear Energy*, 136, 107011. <https://doi.org/10.1016/j.anucene.2019.107011>
- [35] C. Fecarotti, J. Andrews, R. Chen, A Petri net approach for performance modelling of polymer electrolyte membrane fuel cell systems, *International Journal of Hydrogen Energy* 41 (28), 2016, pp12242–12260. doi:10.1016/j.ijhydene.2016.05.138.
- [36] A. Vasilyev, J. Andrews, L. M. Jackson, S. J. Dunnett, B. Davies, Component-based modelling of PEM fuel cells with bond graphs, *International Journal of Hydrogen Energy* 42 (49), 2017, pp29406–29421. doi:10.1016/j.ijhydene.2017.09.004.
- [37] R. O'Hayre, S.-W. Cha, Colella, W. and F. B. Prinz, *Fuel Cell Fundamentals*, 3rd Edition, John Wiley & Sons, 2016.
- [38] F. Barbir, *PEM Fuel Cells: Theory and Practice*, Academic Press, 2013.
- [39] X. Zhang, P. Pisu, Prognostic-oriented Fuel Cell Catalyst Aging Modeling and Its Application to Health-Monitoring and Prognostics of a PEM Fuel Cell, *International Journal of Prognostics and Health Management*, 2014, 1–16.
- [40] M. Chandesris, R. Vincent, L. Guetaz, J. S. Roch, D. Thoby, M. Quinaud, Membrane degradation in PEM fuel cells: From experimental results to semi-empirical degradation laws, *International Journal of Hydrogen Energy* 42 (12), 2017, pp8139–8149. doi:10.1016/j.ijhydene.2017.02.116.
- [41] M. Jouin, R. Gouriveau, D. Hissel, M. C. Pera, N. Zerhouni, Degradations analysis and aging modeling for health assessment and prognostics of PEMFC, *Reliability Engineering and System Safety* 148, 2016, 78–95. doi:10.1016/j.ress.2015.12.003.
- [42] Y. S. Chen, C. W. Yang, J. Y. Lee, Implementation and evaluation for anode purging of a fuel cell based on nitrogen concentration, *Applied Energy* 113, 2014, pp1519–1524. doi:10.1016/j.apenergy.2013.09.028.
- [43] K. D. Baik, M. S. Kim, Characterization of nitrogen gas crossover through the membrane in proton-exchange membrane fuel cells, *International Journal of Hydrogen Energy* 36 (1), 2011, pp732–739. doi:10.1016/j.ijhydene.2010.09.046.
- [44] T. Matsuura, J. Chen, J. B. Siegel, A. G. Stefanopoulou, Degradation phenomena in

- PEM fuel cell with dead-ended anode, *International Journal of Hydrogen Energy* 38 (26), 2013, pp11346–11356. doi:10.1016/j.ijhydene.2013.06.096.
- [45] FC LAB, [IEEE PHM 2014 Data Challenge](http://eng.fcclab.fr/ieee-phm-2014-data-challenge/), 2014. URL <http://eng.fcclab.fr/ieee-phm-2014-data-challenge/>
- [46] M. Fowler, J. Amphlett, Issues associated with voltage degradation in a PEMFC, *Journal of New Materials for Electrochemical Systems* 5, 2002, pp255–262.
- [47] S. Proß, B. Bachmann, PNlib - An Advanced Petri Net Library for Hybrid Process Modeling, *Proceedings 9th Modelica Conference*, Munich, Germany, 2012, pp47–56, doi:10.3384/ecp1207647.
- [48] P. D. T. O'Connor, A. Kleyner, *Practical Reliability Engineering*, John Wiley & Sons, Ltd, Chichester, UK, 2011. doi:10.1002/9781119961260.
- [49] D. J. Smith, *Reliability, Maintainability and Risk*, seventh Edition, Elsevier, 2005.
- [50] T. R. Moss, *The Reliability Data Handbook*, Professional Engineering Publishing, London, 2005.
- [51] N. Noguier, D. Candusso, R. Kouta, F. Harel, W. Charon, G. Coquery, A framework for the probabilistic analysis of PEMFC performance based on multi-physical modelling, stochastic method, and design of numerical experiments, *International Journal of Hydrogen Energy* 42 (1), 2017, pp459–477. doi:10.1016/j.ijhydene.2016.11.074.